JOURNAL OF SOLID STATE CHEMISTRY **136,** 8–15 (1998)
ARTICLE NO. SC977599

On the $Li_xNi_{0.8}Co_{0.2}O_2$ System

I. Saadoune[1] and C. Delmas[2]

Institut de Chimie de la Matière Condensée de Bordeaux, CNRS, and Ecole Nationale Supérieure de Chimie et Physique de Bordeaux, Av. Dr. A. Schweitzer, 33608 Pessac Cedex, France

Received May 14, 1997; in revised form August 11, 1997; accepted August 19, 1997

$Li_xNi_{0.8}Co_{0.2}O_2$ phases ($0.4 \leq x \leq 1.0$) have been obtained by electrochemical deintercalation from 2D $LiNi_{0.8}Co_{0.2}O_2$. X-ray diffraction shows that, contrary to what is observed for Li_xNiO_2, there is no phase transition during lithium deintercalation, in good agreement with the electrochemical behavior. The physical properties (magnetic susceptibility, electronic conductivity, and thermoelectronic measurements) show that nickel ions are predominantly oxidized to the tetravalent state. The good reversibility of the lithium intercalation process, due to the strictly 2D character of the $Li_xNi_{0.8}Co_{0.2}O_2$ materials, the high cell voltage (but not too high due to the position of the Ni^{4+}/Ni^{3+} couple vs the Co^{4+}/Co^{3+} couple), and the presence of a relatively small cobalt content, makes this material a very promising one for some lithium battery applications.

INTRODUCTION

A_xMO_2 lamellar oxides (A = Li, Na and $M = 3d$ element) have been intensively studied as a result of their anisotropic character, which leads to very interesting physical and electrochemical properties (1–4). Their recent utilization as positive electrode materials in high energy density batteries also explains the large number of studies devoted to these materials (5–8). Their electrochemical and physical properties depend strongly on the nature of the transition metal ion, its oxidation state, and the nature of the chemical bonding within the $(MO_2)_n$ slabs.

A few years ago, we have investigated the $LiNiO_2$–$LiCoO_2$ solid solution with the aim of selecting a promising $LiNi_{1-y}Co_yO_2$ material for possible application in rocking chair batteries (9–11). This work in fact constituted the first step in a large series of studies concerning this solid solution. Most of the studies reported in this field are concerned with the electrochemical behavior of these materials in lithium batteries (12–14). Only a few of them are devoted to studies of the physical property modifications related to lithium deintercalation.

Considering the lithium nickelate, it is well known that its true formula is $Li_{1-z}Ni_{1+z}O_2$ ($z \geq 0.02$) and, therefore, contains simultaneously Ni^{3+} and Ni^{2+} ions. During lithium deintercalation, the Fermi level is displaced from the Ni^{3+}/Ni^{2+} redox couple to the Ni^{4+}/Ni^{3+} one with an important modification in the physical properties (15, 16). Substitution of cobalt for nickel reduces the excess of nickel ions and, therefore, leads to the presence of only one oxidation state for the transition metal ions in the $LiNi_{1-y}Co_yO_2$ starting phases ($y \geq 0.2$) (17). Therefore, a question arises: during lithium deintercalation, is there a selective oxidation of cobalt or nickel and what are the effects on the physical properties?

The general aim of our work is to show the effect of lithium extraction from $LiNi_{1-y}Co_yO_2$ phases on the structural and physical properties. We have selected two starting compositions ($y = 0.2$ and $y = 0.9$) which seem to be representative of the general behavior of this system. The structural, electrochemical, and physical studies of the $Li_xNi_{0.8}Co_{0.2}O_2$ nickel-rich phases are presented in the present paper. The results obtained for the $Li_xNi_{0.1}Co_{0.9}O_2$ cobalt-rich phases will be reported in a forthcoming paper.

EXPERIMENTAL

The $LiNi_{0.8}Co_{0.2}O_2$ starting phase was obtained by direct reaction of NiO, Co_3O_4, and Li_2CO_3 in stoichiometric proportions. Several thermal treatments (600°C for 24 h and then 48 h at 800°C under dry oxygen) were necessary to obtain a pure phase.

Electrochemical studies were carried out with $Li/LiClO_4$ in propylene carbonate/$Li_xNi_{0.8}Co_{0.2}O_2$ cells. For classical electrochemical experiments, the positive electrode consisted of a mixture of 90% by weight active material and 10% ketjenblack. In the case of the electrochemical preparation of partially deintercalated phases for physical characterization, the pure $LiNi_{0.8}Co_{0.2}O_2$ phase was used without carbon as an electronic conductor. In the case of materials prepared for the electronic properties study, sintered pellets

[1] Permanent address: Université Cadi Ayyad, FST Marrakech, BP 618, Marrakech, Morocco.

[2] To whom correspondence should be addressed.

0022-4596/98 $25.00

(3 tons for a diameter of 0.8 cm followed by a thermal treatment of 12 h at 800°C under oxygen) of the starting phase were used as the positive electrode. The cells, assembled in an argon-filled dry box, were charged under very low current density (70 $\mu A/cm^2$). In these conditions, the cell polarization is very small. When the desired lithium amount is reached, the cell stays in open circuit to obtain a complete material homogenization. The open circuit voltage (OCV) values obtained in these conditions are very close to those obtained in classical OCV experiments. Therefore, one can assume that the pellets exhibit a good homogeneity. Moreover, as discussed in the following, due to the absence of structural transition and to the small changes in lattice parameters, there is no damage in the pellets. Therefore, one can consider that the results of the electronic properties study are completely relevant. For the thermodynamic potential measurements (open circuit voltage), the charge process was interrupted by relaxation periods. To be as close as possible to the equilibrium conditions, the relaxation periods were interrupted when the slope of the voltage–time curve was smaller than 0.1 mV/h. After deintercalation, the positive electrode materials were analyzed by X-ray diffraction before any physical measurements.

The X-ray diffraction (XRD) patterns were obtained with an INEL CPS 120 curve position sensitive detector using a cobalt anticathode. To prevent any reaction with air moisture, all XRD experiments were performed in sealed capillaries (under dry argon). Magnetic susceptibility measurements were obtained from 4 to 300 K, using an automatic susceptometer (DSM 8, Manics). Electrical conductivity measurements were carried out with the four-probe direct-current method in the 100–300 K temperature range. The thermoelectronic power measurements were performed in the same temperature range with homemade equipment (18).

RESULTS AND DISCUSSION

The X-ray diffraction pattern of the $LiNi_{0.8}Co_{0.2}O_2$ starting phase shows a rhombohedral symmetry with the so-called O3 structural type (19) (space group $R\bar{3}m$): The lattice is built up by edge-sharing $(Ni_{0.8}Co_{0.2})O_6$ octahedra forming layers and the lithium ions are located in octahedral (O) sites between the layers. The number 3 indicates the existence of three slabs per hexagonal cell. This structure is schematically represented in Fig. 1. As previously reported, Rietveld refinement of the X-ray pattern shows that the amount of nickel within the lithium plane is very small ($z = 0.010(5)$ in $Li_{1-z}Ni_{0.8+z}Co_{0.2}O_2$) (17). Therefore, in the present work, the ideal formula is used.

Electrochemical Study

The $LiNi_{0.8}Co_{0.2}O_2$ phase has been used as the positive electrode in lithium batteries. The evolution of the cell voltage of the $Li//Li_xNi_{0.8}Co_{0.2}O_2$ cell with the lithium amount is shown in Fig. 2 for the first cycle obtained with charge and discharge interrupted by relaxation periods.

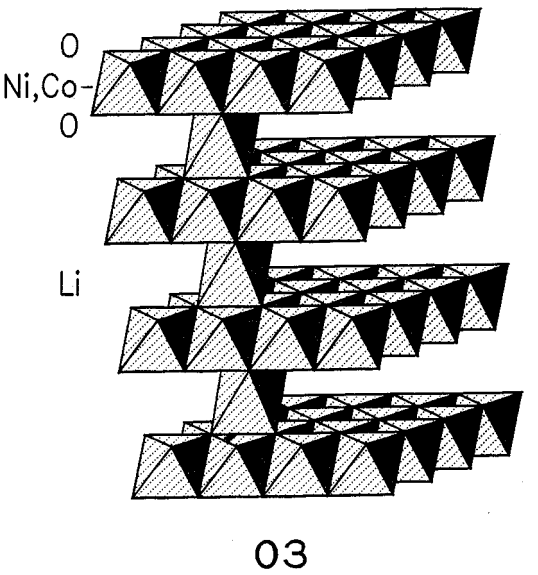

FIG 1. Schematic representation of the $LiNi_{0.8}Co_{0.2}O_2$ structure.

The polarization of this battery, given by the height of vertical lines in the $V = f(x)$ plot, is very low over the whole composition range, indicating a very high lithium diffusion kinetics in the interslab space. We should point out that the polarization slightly increases during discharge as x increases. As shown in the inserts of Fig. 2 ($V = f(t)$ plots), for the very deintercalated phases, thermodynamic equilibrium is reached after a few hours, while for the more intercalated phases, the relaxation duration becomes longer as a result of the decreasing thickness of the interslab space during lithium intercalation as discussed in the following. It should be noticed that the $LiNi_{0.8}Co_{0.2}O_2$ starting phase is not totally restored during the lithium reintercalation reaction. This phenomenon, very general in lithium batteries, is mainly due to the increasing lithium–lithium electrostatic repulsion when x becomes close to one. The similarity between the charge and discharge curves indicates a very good reversibility.

The almost monotonous variation of the potential–composition curve reflects the existence of a solid solution domain over the whole $0.4 \leq x \leq 1.0$ composition range, which is in good agreement with X-ray diffraction results discussed in the next section. This result differs from that shown in the Li_xNiO_2 system (20, 21). The derivative of the cycling curve, $-dx/|dV| = f(x)$, is plotted in Fig. 3 in comparison with that obtained in the Li_xNiO_2 system (22). The strong peaks in the derivative curve associated with the biphased domains of Li_xNiO_2 have disappeared in the mixed Ni–Co system. Nevertheless, the shape of the curve,

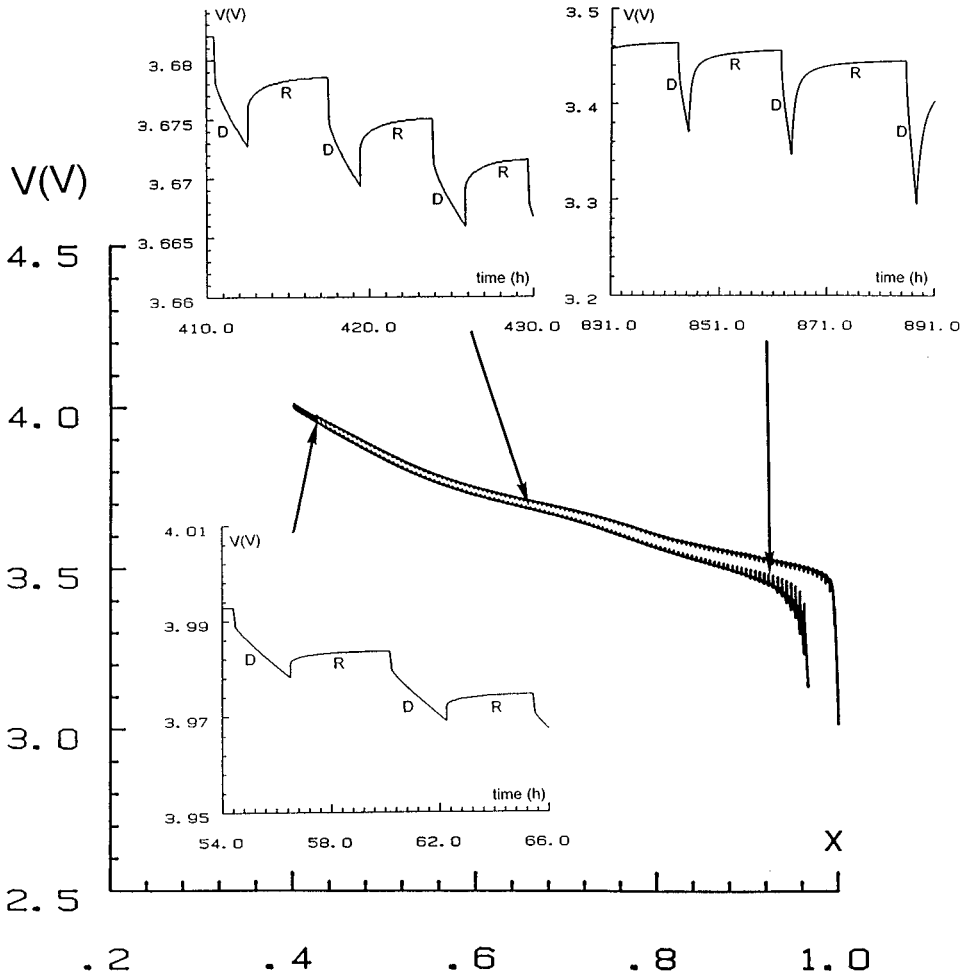

FIG 2. First galvanostatic intermittent charge–relaxation and discharge–relaxation cycle of an $Li//Li_xNi_{0.8}Co_{0.2}O_2$ cell ($J = 70\ \mu A/cm^2$; relaxation criterion: $\Delta x/h = 0.1$ mV/h).

which is characteristic of the existence of two adjacent solid solution domains (23), suggests that a special behavior must exist in the vicinity of the $x = 0.75$ composition.

The experimental energy recovered on continuous discharge of the $Li//Li_xNi_{0.8}Co_{0.2}O_2$ cell is close to 500 W h/kg (of active material) (10). This justifies the particular interest of several battery companies and many electrochemical researchers for this type of lamellar oxide (24, 25).

X-Ray Characterization

The X-ray diffraction patterns of the $Li_xNi_{0.8}Co_{0.2}O_2$ samples removed from the electrochemical cell after lithium deintercalation are shown in Fig. 4. All patterns exhibit narrow diffraction lines, showing that the good crystallinity is preserved during the electrochemical cycling. The similarity between all X-ray diffraction patterns shows that the rhombohedral symmetry is preserved during lithium deintercalation from the $LiNi_{0.8}Co_{0.2}O_2$ oxide. For the "$LiNiO_2$" unsubstituted phase, crystal structure changes have been evidenced upon lithium deintercalation by the research groups of Ohzuku (20) and Dahn (21). The rhombohedral symmetry of the pristine "$LiNiO_2$" nickelate transforms into a monoclinic symmetry in a large $0.35 < x < 0.75$ composition range (22). Recent studies performed in our laboratory by Pérès *et al.* for the $Li_{0.63}Ni_{1.02}O_2$ composition have shown, from X-ray diffraction, EXAFS, and electron diffraction, that the driving force of the monoclinic distortion is not the Jahn–Teller effect of trivalent nickel (26) but a lithium–vacancy ordering which leads to a superstructure (27). For the $Li_xNi_{0.8}Co_{0.2}O_2$ cobalt-substituted phases, one could assume that the presence of cobalt ions (20%) in the $(NiO_2)_n$ slabs impedes this lithium–vacancy ordering, leading to the maintenance of the rhombohedral symmetry in the studied ($0.5 \leq x \leq 1.0$) composition domain. Nevertheless, the peculiar behavior observed in the $-dx/|dV|$ vs x curve (Fig. 3) around the

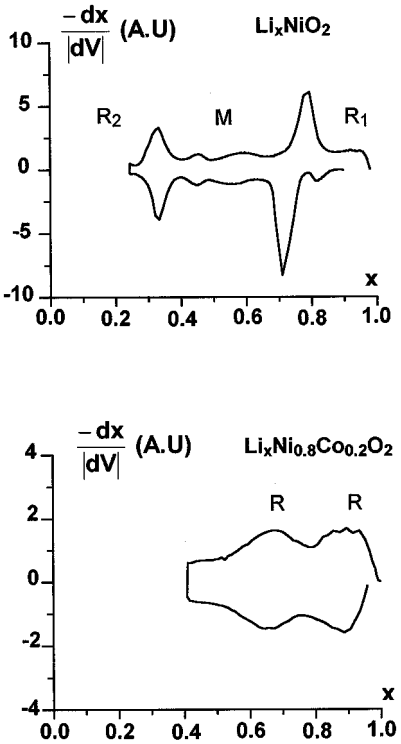

FIG 3. Comparison of the derivative curves, $-dx/|dV| = f(V)$, of the $Li//Li_xNiO_2$ and $Li//Li_xNi_{0.8}Co_{0.2}O_2$ cells (R, R_1, R_2 : rhombohedral symmetry; M: monoclinic symmetry).

$x = 0.75$ composition suggests that correlations between lithium ions would tend to an ordered distribution. One can think that the presence of a large amount of cobalt within the slabs prevents a long-range Li^+ ion ordering and, therefore, any structural distortion.

The variation vs x of the splitting between the (018) and (110) diffraction lines emphasizes that the hexagonal cell parameters change during the electrochemical cycling. Figure 5 reports the evolution of the hexagonal cell parameters, refined by the least-squares method, of the $Li_xNi_{0.8}Co_{0.2}O_2$ phases. The a_{hex} parameter, which is related to the metal–metal intraslab distance, decreases upon lithium deintercalation as a result of the appearance of tetravalent transition metal ions. The increase of the c_{hex} parameter as x decreases clearly reflects the competition

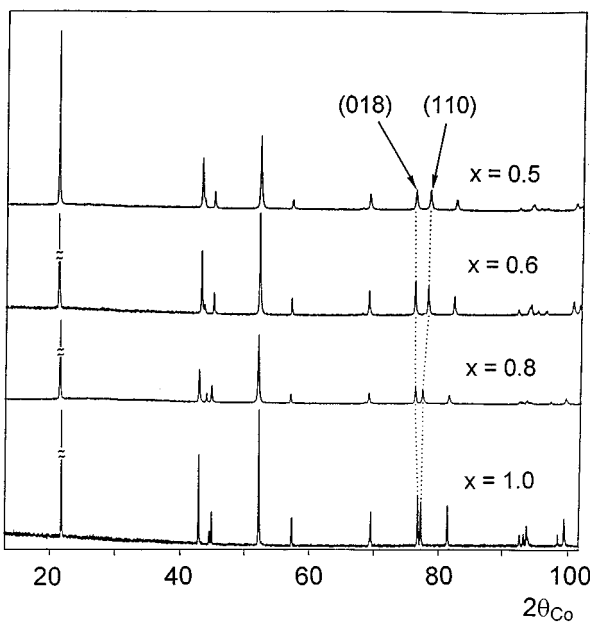

FIG 4. X-ray diffraction patterns of the $Li_xNi_{0.8}Co_{0.2}O_2$ phases.

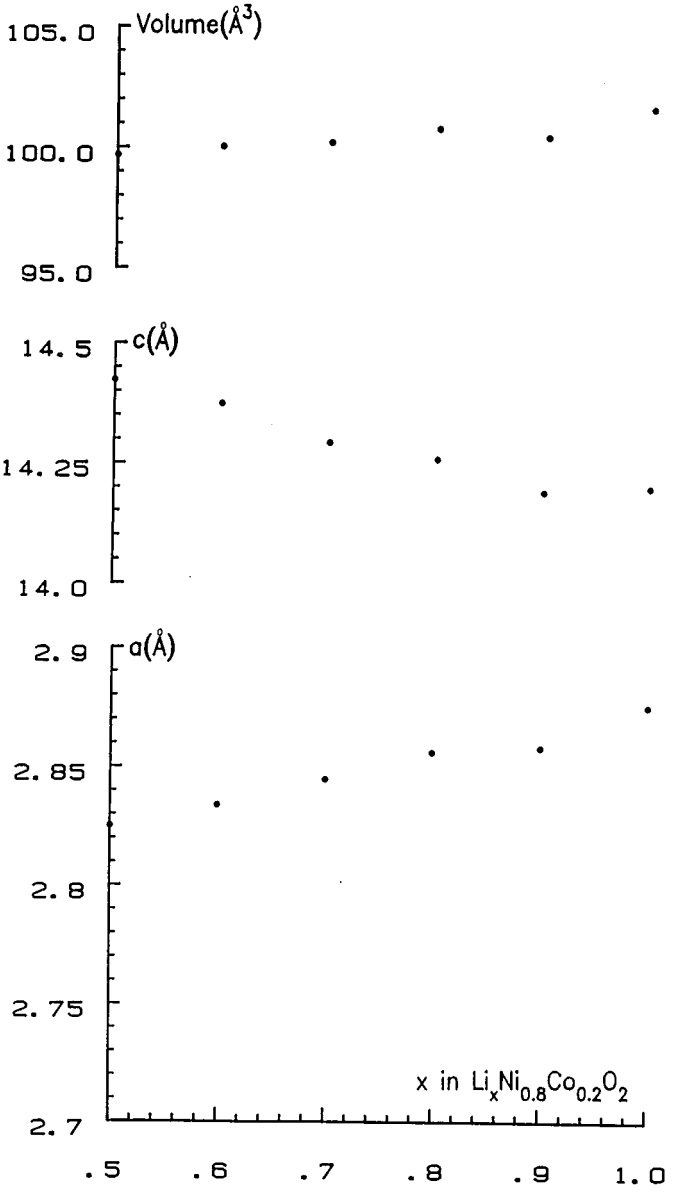

FIG 5. Variation of the hexagonal cell parameters and the cell volume for the $Li_xNi_{0.8}Co_{0.2}O_2$ phases as a function of the lithium amount.

between the interslab electrostatic repulsions and the electrostatic attraction resulting from the presence of lithium ions between the slabs. In this case, the steric effect due to the increase of the number of lithium ions does not play a significant role. This latter evolution is in contrast with that observed for A_xMS_2 layered chalcogenides in which the variation of the interslab distance is mainly related to steric effects as a result of the high M–S covalency which makes secondary the electrostatic effects (28, 29). It is also important to note that the hexagonal cell volume varies very slightly in the studied composition domain (about 2%). This result is very important for applications as the long-range cycling behavior must depend on the volume variations of the active electrode material which induce strains within the electrode and, therefore, can lead to a significant loss of cell capacity.

Magnetic Properties Study

With the aim of knowing the nature of the transition metal ion (Ni^{3+} or Co^{3+}) that is oxidized during lithium deintercalation, a magnetic study of the $Li_xNi_{0.8}Co_{0.2}O_2$ phases was carried out. Figure 6 shows the thermal variation of the reciprocal magnetic molar susceptibility for $x = 1.0$, 0.9, 0.8, and 0.65.

For the $LiNi_{0.8}Co_{0.2}O_2$ starting phase, the linearity of the $1/\chi_m$ vs T curve is typical of a Curie–Weiss paramagnetism. It reflects the localization of the magnetic moments in this material. A fit of the curve in the 100–300 K paramagnetic domain clearly shows that the trivalent nickel and cobalt ions have low-spin configurations. This result is in good agreement with the short M–O distance (1.967 Å) found in the Rietveld refinement analysis of the $LiNi_{0.8}Co_{0.2}O_2$ X-ray diffraction pattern (17). The positive value of the paramagnetic Curie temperature shows the predominance of the ferromagnetic coupling due to the 90° Ni–O–Ni interaction within the $(Ni_{0.8}Co_{0.2}O_2)_n$ slabs. This behavior is different from that observed for $LiNiO_2$. This latter oxide exhibits a ferrimagnetic behavior due to the presence of a small amount of divalent nickel ions in the lithium layer (30). This remark confirms a detailed structural study of the $LiNi_{1-y}Co_yO_2$ system which reports that substitution of cobalt for nickel tends to increase the 2D structural character of this system (17).

For the oxidized $Li_xNi_{0.8}Co_{0.2}O_2$ phases, a similar magnetic behavior was observed. Nevertheless, the magnetic moment decreases with decreasing lithium amount. The variation of the Curie constant (C_{exp}) with x is compared in Table 1 with the theoretical values calculated in two limit hypotheses: oxidation of nickel (C_1) and oxidation of cobalt

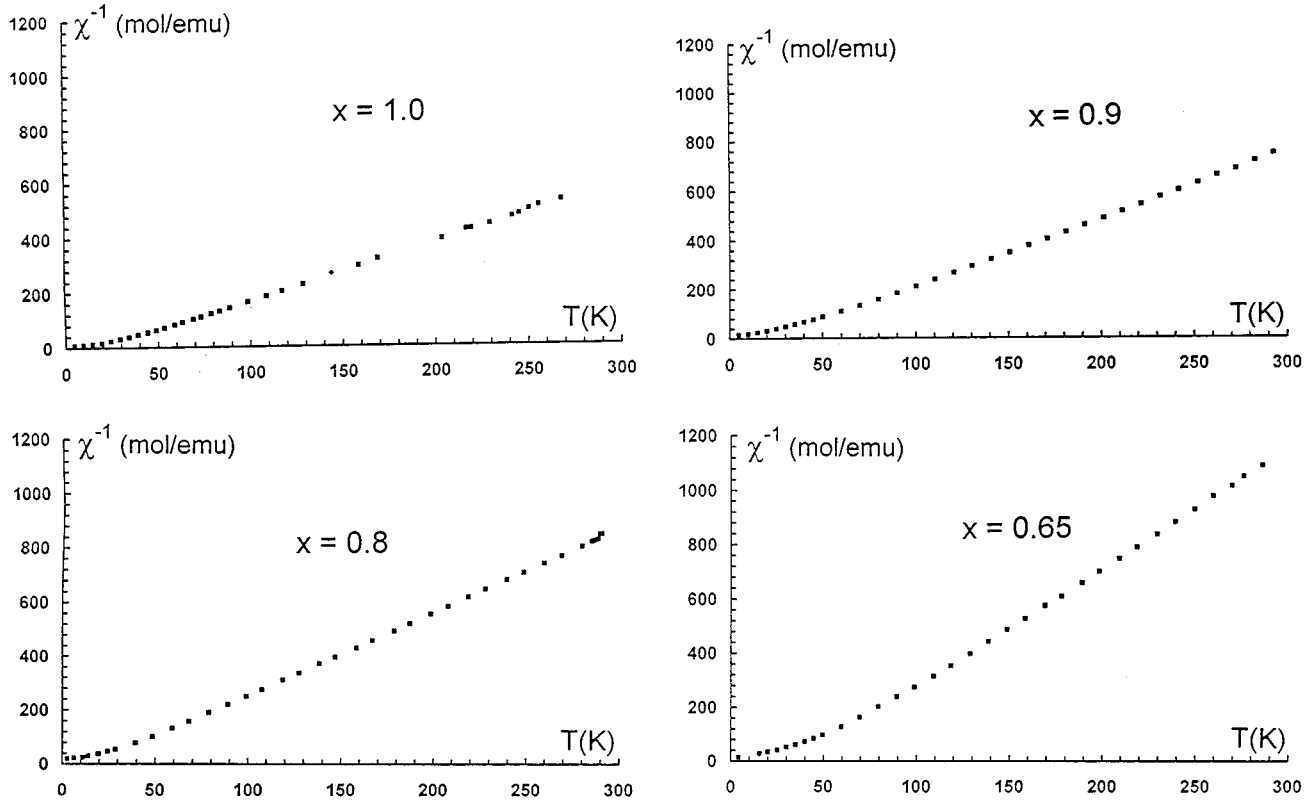

FIG 6. Thermal variation of the reciprocal magnetic molar susceptibility of the $Li_xNi_{0.8}Co_{0.2}O_2$ phases.

TABLE 1
Comparison of the Experimental (C_{exp}) and Theoretical Curie Constants of $Li_xNi_{0.8}Co_{0.2}O_2$[a]

x	C_{exp}	C_1	C_2
1.0	0.47	0.30	0.30
0.9	0.37	0.26	0.34
0.8	0.32	0.22	0.38
0.65	0.23	0.17	0.32

[a] C_1, Curie constant calculated in the hypothesis of the oxidation of Ni^{3+}; C_2, Curie constant calculated in the hypothesis of the oxidation of Co^{3+}.

(C_2). Although a small difference is observed between the experimental values and the calculated ones under the nickel oxidation hypothesis, the variation looks similar. A very different variation is observed in the case of the cobalt oxidation hypothesis. Therefore, these results suggest that low-spin Ni^{3+} ions ($t_2^6 e^1$) are preferentially oxidized to low-spin diamagnetic Ni^{4+} ions ($t_2^6 e^0$). This can be explained if one considers the relative instability of the nickel e^1 electron, which occupies an antibonding σ^*_{Ni-O} molecular orbital, compared to the cobalt t_2^6 ones. A similar result has been obtained on the γ-oxyhydroxides with general formula $H_xK_w(H_2O)_zNi_{1-y}Co_yO_2$ in which the average oxidation level of transition metals is close to 3.5 (31). These oxyhydroxides, which can be used as the positive electrode in Ni–Cd generators, contain only Ni^{3+}, Co^{3+}, and Ni^{4+} ions for $y \leq 0.4$ and a small amount of Co^{4+} for $y > 0.4$.

Electrical Properties Study

The foregoing results suggest that trivalent nickel ions are preferentially oxidized to the tetravalent state, rather than cobalt ions. To unambiguously confirm this behavior, a detailed study of the electronic transport properties was carried out. From a general point of view, nickel oxidation must lead to a small polaron type conductivity, while cobalt oxidation must lead to a tendency to electronic delocalization through the direct t_2–t_2 overlapping.

Electrical conductivity. The variation of the electrical conductivity vs reciprocal temperature for the $Li_xNi_{0.8}Co_{0.2}O_2$ phases is shown in Fig. 7. Over the entire composition range, the electrical conductivity shows an activated character with a slight change in the curve slope. This thereby confirms the electronic localization in these phases. The activation energy values, calculated using an Arrhenius law in two temperature domains, are typical for the small polaron conduction phenomenon generally observed in mixed-valence systems (Table 2). This result is in good agreement with the presence of Ni^{4+} ions in the material and, therefore, of a Ni^{3+}–O^{2-}–Ni^{4+} hopping. For Ni^{3+}, Co^{3+}, and Ni^{4+} ions, all three (t_2) orbitals are filled. Therefore, although the metal–metal distance (equal to the a_{hex} parameter) becomes smaller than the critical distance, given by Goodenough's formula (32), upon lithium deintercalation ($R_c = 2.85$ Å for $x = 1.0$ and $R_c = 2.87$ Å for $x = 0.5$), no electronic delocalization can be expected.

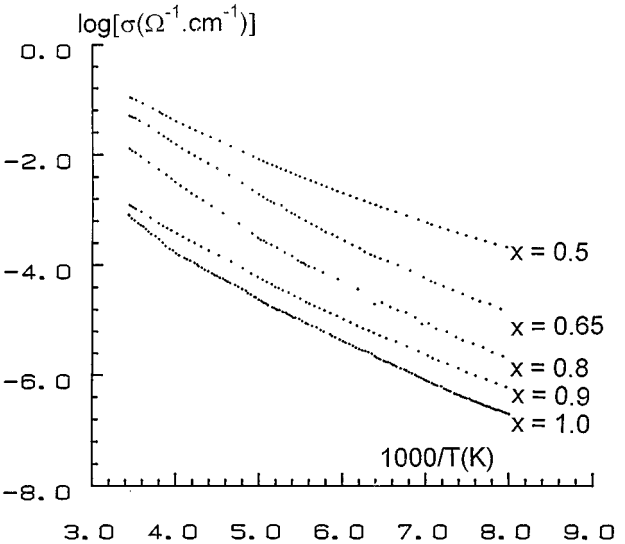

FIG 7. Variation of the electrical conductivity vs reciprocal temperature of the $Li_xNi_{0.8}Co_{0.2}O_2$ phases.

The observed electronic localization indicates that, even if some cobalt ions are oxidized to the tetravalent state, their number must be very small since a significant amount would entail a metallic behavior due to the presence of holes in the broad t_2 band.

The increase of the electrical conductivity at room temperature during lithium deintercalation results from (i) the increasing number of Ni^{4+} ions, which leads to holes in the narrow "Ni^{4+}/Ni^{3+}" band, and (ii) the decrease of the Ni^{4+}–O^{2-} distance resulting from a higher covalency, which makes the Ni^{3+}–O^{2-}–Ni^{4+} hopping easier.

TABLE 2
Activation Energies for the Electronic Conductivity of the $Li_xNi_{0.8}Co_{0.2}O_2$ Phases Calculated in the 125–170 and 220–290 K Temperature Domains

	Activation energy (eV)	
x in $Li_xNi_{0.8}Co_{0.2}O_2$	125–170 K temperature domain	220–290 K temperature domain
1.0	0.11	0.22
0.9	0.11	0.18
0.8	0.13	0.20
0.65	0.11	0.17
0.5	0.08	0.16

Thermoelectronic power measurements. Because of the relatively high resistance of the $Li_xNi_{0.8}Co_{0.2}O_2$ materials, thermoelectronic power measurements were restricted to the 100–300 K temperature range for all studied compositions ($x = 0.9$, 0.8, 0.65, 0.5). As shown in Fig. 8, the thermoelectronic power exhibits positive values for $x \geq 0.65$, whereas for the $Li_{0.5}Ni_{0.8}Co_{0.2}O_2$ phase, the Seebeck coefficient becomes negative. This indicates a change in the charge carriers during lithium extraction. For all studied compositions, the thermoelectronic power is almost independent of temperature. This behavior is typical of a small polaron type transport mechanism, where there is no thermal activation of the number of carriers. Moreover, the decrease in the absolute value of the Seebeck coefficient in the $0.65 \leq x \leq 0.9$ range clearly emphasizes the increase of the number of charge carriers upon deintercalation.

As previously proposed for $NaNiO_2$ (33), the schematic energy vs density of state $N(E)$ diagram shown in Fig. 9 can be proposed (Fig. 9). Intraatomic electrostatic interaction between localized electrons introduces an energy gap between successive redox energies corresponding to Ni^{3+}/Ni^{2+} and Ni^{4+}/Ni^{3+} couples. For low-spin trivalent cobalt ions, the "t_2" band is completely filled (t_2^6). Since these ions are not oxidized during the electrochemical oxidation, one can assume that its energy level is lower than that of the narrow band associated with the Ni^{4+}/Ni^{3+} redox couple. One can also assume that the O^{2-} $2p^6$ band and the "t_2" nickel band have lower energies than the top of the "t_2" cobalt band. As schematically shown in Fig. 9, if more than 0.8 lithium were removed from the $LiNi_{0.8}Co_{0.2}O_2$ phase, holes must be created in the cobalt "t_2^6" band in a first step, and maybe in the O $2p$ band for the larger deintercalation amounts.

For the starting $LiNi_{0.8}Co_{0.2}O_2$ composition, the Ni^{4+}/Ni^{3+} band is filled and the Fermi level lies between the two redox couples (Fig. 9). During lithium deintercalation, the nickel oxidation leads to a small polaron conductivity. For $x > 0.6$, electron holes are the predominant charge carriers (the Seebeck coefficient is positive), while for $x < 0.6$, the narrow Ni^{4+}/Ni^{3+} band is less than half filled and electrons are the main charge carriers ($\alpha < 0$). This change in the nature of the predominant charge carriers is also in agreement with the preferential oxidation of nickel vs cobalt. Indeed, if a significant amount of cobalt ions were oxidized during the lithium deintercalation, both bands (the Ni^{4+}/Ni^{3+} and the $(t_2^6)_{Co}$ ones) would remain more than half filled and the Seebeck coefficient would be positive.

This discussion about the electronic properties of oxides must consider the possible existence of an oxygen departure from stoichiometry. In layered oxides, oxygen non-stoichiometry has only been evidenced in sodium cobalt oxides with a large amount of tetravalent cobalt ions (34). In the case of layered lithium ternary oxides, such departure has never been reported. Even if it occurs, it would be very small; therefore, the number of electrons involved would be very small in comparison to that induced by the lithium deintercalation. Moreover, since all deintercalation reactions are realized at room temperature, the (Ni + Co)/O ratio remains unmodified. Therefore, all the changes observed in electronic properties result from the oxidation due to the lithium deintercalation.

CONCLUSION

Structural characterization of the $Li_xNi_{0.8}Co_{0.2}O_2$ phases shows that electrochemical cycling of the

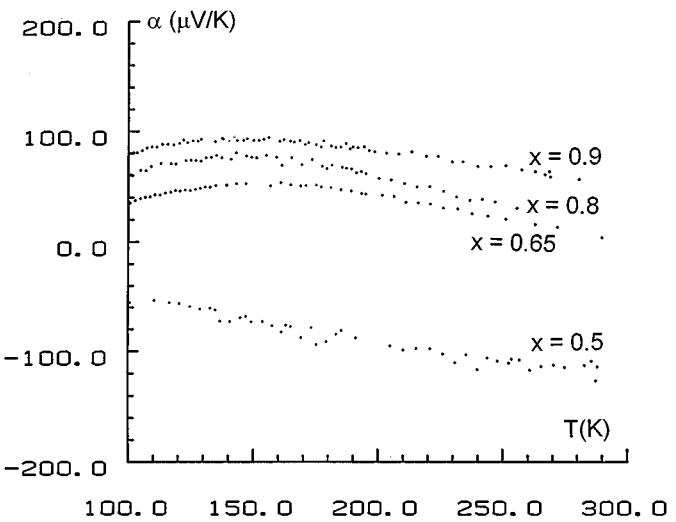

FIG 8. Thermal variation of the Seebeck coefficient of the $Li_xNi_{0.8}Co_{0.2}O_2$ phases.

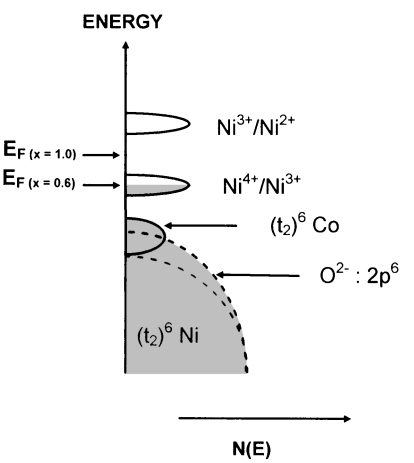

FIG 9. Schematic energy vs density of state diagram of $Li_xNi_{0.8}Co_{0.2}O_2$ materials showing the evolution of the Seebeck coefficient sign. In this scheme, the Co^{3+}/Co^{2+} redox couple, which exhibits a higher energy than the Ni^{3+}/Ni^{2+} one, is not represented.

$Li//Li_xNi_{0.8}Co_{0.2}O_2$ cell occurs without any change in the crystal symmetry, contrary to what is observed in the Li_xNiO_2 system. This difference results from the presence of a large amount of cobalt ions, which prevent any long-range lithium–vacancy ordering within the interslab space. Moreover, a detailed physical properties study of $Li_xNi_{0.8}Co_{0.2}O_2$ phases has evidenced that only nickel ions are oxidized to the tetravalent state upon lithium deintercalation. Thus, electronic conductivity measurements have demonstrated that the conduction mechanism results from a Ni^{3+}–O^{2-}–Ni^{4+} hopping. The room temperature electronic conductivity, which is significantly high in the pristine phase, increases rapidly upon lithium deintercalation. Moreover, the increase of the interslab thickness when lithium is removed must make lithium diffusion easier. Both contributions lead to a very small cell polarization during cycling. The electrochemical process, which involves only the Ni^{4+}/Ni^{3+} redox couple, decreases significantly the cell voltage as compared to $LiCoO_2$ and therefore avoids some electrolyte stability problems. Versus $LiNiO_2$, this material seems to exhibit some advantages: the structural transitions are suppressed and, moreover, the 2D character resulting from the presence of cobalt allows an almost complete lithium reintercalation and therefore increases the cell capacity. Therefore, one can think that this material can compete with $LiCoO_2$ for main applications and with $LiNiO_2$ for small-cell applications.

ACKNOWLEDGMENTS

The authors wish to thank J. B. Goodenough for fruitful discussions and CNES and Region Aquitaine for financial support.

REFERENCES

1. T. A. Hewston and B. Chamberland, *J. Phys. Chem. Solids* **48,** 97 (1987).
2. C. Delmas, G. Le Flem, C. Fouassier, and P. Hagenmuller, *J. Phys. Chem. Solids* **39,** 155 (1978).
3. E. Rossen, C. W. Jones, and J. R. Dahn, *Solid State Ionics* **57,** 311 (1992).
4. J. P. Kemp and P. A. Cox, *J. Phys.: Condens. Matter*, **2,** 9653 (1990).
5. K. Mizushima, P. C. Jones, P. J. Wiseman, and J. B. Goodenough, *Mater Res. Bull.* **15,** 783 (1980).
6. M. G. S. R. Thomas, W. I. F. David, J. B. Goodenough, and P. Groves, *Mat. Res. Bull.* **20,** 1137 (1985).
7. J. N. Reimers and J. R. Dahn, *J. Electrochem. Soc.* **139,** 2091 (1992).
8. M. Broussely, F. Perton, P. Biensan, J. M. Bodet, A. Lecerf, C. Delmas, A. Rougier, and J. P. Pérès, *J. Power Sources* **54,** 54 (1995).
9. C. Delmas and I. Saadoune, *Solid State Ionics* **53–56,** 370 (1992).
10. C. Delmas, I. Saadoune, and A. Rougier, *J. Power Sources* **43–44,** 595 (1993).
11. I. Saadoune and C. Delmas, *J. Mater. Chem.* **6**(2), 193 (1996).
12. A. Ueda and T. Ohzuku, *J. Electrochem. Soc.* **141**(8), 2010 (1994).
13. T. Ohzuku, K. Sawai, A. Ueda, M. Nagayama, Y. Iwakoshi, and H. Komori, *Electrochim. Acta* **38,** 1159 (1993).
14. R. Alcantaro, J. Morales, T. L. Tirado, R. Stoyanova, and E. Zhecheva, *J. Electrochem. Soc.* **142**(12), 3997 (1995).
15. G. Dutta, A. Manthiram, J. C. Grenier, and J. B. Goodenough, *J. Solid State Chem.* **96,** 123 (1993).
16. R. Stoyanova, E. Zhecheva, and C. Friebel, *J. Phys. Chem. Solids* **54**(1), 9 (1993).
17. A. Rougier, I. Saadoune, P. Gravereau, P. Willmann, and C. Delmas, *Solid State Ionics* **90,** 83 (1996).
18. P. Dordor, E. Marquestau, and G. Villeneuve, *Rev. Phys. Appl.* **15,** 1607 (1980).
19. C. Delmas, J. J. Braconnier, C. Fouassier, and P. Hagenmuller, *Solid State Ionics* **3–4,** 165 (1981).
20. T. Ohzuku, A. Ueda, and M. Nagayama, *J. Electrochem. Soc.* **140,** 1862 (1993).
21. W. Li, J. N. Reimers, and J. R. Dahn, *Solid State Ionics* **67,** 123 (1993).
22. J. P. Pérès, Thesis, University of Bordeaux I, France, 1996.
23. M. B. Armand, Thesis, University of Grenoble, France, 1978.
24. Y. Nishi, H. Azuma, and A. Omaru, U.S. Patent, 4,959,281, Sept. 25, 1990.
25. A. Lecerf, M. Broussely, and J. P. Gabano, European Patent Application EP 89110158, 1989.
26. J. P. Pérès, A. Demourgues, and C. Delmas, *Solid State Ionics*, in press.
27. J. P. Pérès, F. Weill, and C. Delmas, *Solid State Ionics.* [submitted]
28. M. S. Whittingham and A. H. Thompson, *J. Chem. Phys.* **62**(4), 1588 (1975).
29. J. Rouxel, M. Danot, and J. Bichon, *Bull. Soc. Chim. Fr.* 3930 (1977).
30. A. Rougier, C. Delmas, and G. Chouteau, *J. Phys. Chem. Solids* **57**(5–6), 1101 (1996).
31. Y. Borthomieu, Thesis, University of Bordeaux I, France, 1990.
32. J. B. Goodenough, *in* "Progress in Solid State Chemistry" (Reiss, H., Ed.), Vol. 5, p. 279 Pergamon Press, Oxford, 1971.
33. C. Delmas, I. Saadoune, and P. Dordor, *Mol. Cryst. Liq. Cryst.* **244,** 337 (1994).
34. J. Molenda, C. Delmas, P. Dordor, and A. Stoklosa, *Solid State Ionics* **12,** 473 (1984).